

Detecting algorithmic bias in medical-AI models using trees

Jeffrey Smith^{1,*}, Andre Holder², Rishikesan Kamaleswaran³, and Yao Xie¹

¹School of Industrial and Systems Engineering, Georgia Institute of Technology, Atlanta, GA, 30332, USA

²Department of Biomedical Informatics, Emory University School of Medicine, Atlanta, GA, 30303, USA

³Department of Surgery, Duke University School of Medicine, Durham, NC 27708, USA

*jsmith312@gatech.edu

ABSTRACT

With the growing prevalence of machine learning and artificial intelligence-based medical decision support systems, it is equally important to ensure that these systems provide patient outcomes in a fair and equitable fashion. This paper presents an innovative framework for detecting areas of algorithmic bias in medical-AI decision support systems. Our approach efficiently identifies potential biases in medical-AI models, specifically in the context of sepsis prediction, by employing the Classification and Regression Trees (CART) algorithm. We verify our methodology by conducting a series of synthetic data experiments, showcasing its ability to estimate areas of bias in controlled settings precisely. The effectiveness of the concept is further validated by experiments using electronic medical records from Grady Memorial Hospital in Atlanta, Georgia. These tests demonstrate the practical implementation of our strategy in a clinical environment, where it can function as a vital instrument for guaranteeing fairness and equity in AI-based medical decisions.

1 Introduction

The increasing prevalence of machine learning (ML) and artificial intelligence (AI) integration in critical industries like healthcare has ushered in a new era of medical decision-support tools. These systems are characterized by advancements in precision diagnosis, personalized treatment, and enhanced patient care^{1,2}. Although these advancements have the potential to transform the healthcare sector, their use also gives rise to significant ethical considerations, particularly with hidden biases, both social and statistical, that may be embedded in the training data used to develop medical-AI models. As a result, integration of these technologies has created an urgent need to detect hidden bias, particularly in relation to the concept of fairness for medical-AI models. Recently, there has been a growing emphasis on the development of more trustworthy AI and ML systems that prioritize trustworthiness and fairness. Consequently, there are at least 21 distinct mathematical definitions of fairness in existence today³.

Societal biases, from a clinical perspective, can be observed in two primary categories: explicit bias and implicit bias. Explicit biases refer to consciously held views and opinions of healthcare personnel, which directly result in differential treatment depending on particular characteristics of patients, such as race, ethnicity, or age^{4,5}. Conversely, implicit biases are subconscious prejudices that subtly but significantly influence clinical practices and decision-making, often avoiding straightforward identification and regulation⁵⁻⁸. Although efforts have been made to eliminate explicit biases in the healthcare space, the impact of implicit biases on patient-provider interactions and outcomes remains prevalent⁴. These biases are of the utmost importance as they directly impact the data that serves as the foundation for medical-AI models. electronic health record (EHR) data underpinning these systems.

Algorithmic bias poses another significant challenge within the realm of ML and AI systems. This bias commonly emerges as a result of erroneous assumptions made during the training of prediction models, frequently mirroring biases present in the real world or originating from incorrect or insufficient datasets. Within the realm of healthcare, this bias has the potential to result in inaccurate diagnoses or suboptimal interventions, thereby disproportionately affecting particular subgroups of patients and further amplifying pre-existing disparities. The exacerbation of existing disparities in healthcare data is well documented in terms of race⁹⁻¹¹, gender¹², and socio-economic status¹³. Recognition and mitigation of algorithmic bias remain of significant importance, especially in high-stakes situations where patients' lives are at risk⁸.

The critical nature of healthcare decisions, coupled with this nuanced ethical landscape, underscores the urgency of identifying these biases to ensure fair and equitable ML applications in healthcare, especially for diverse and often underrepresented patient sub-populations.

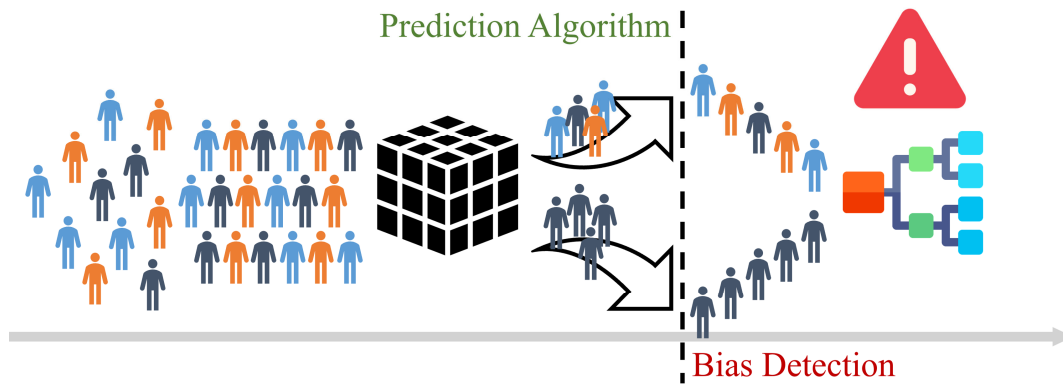


Figure 1. Representation of bias detection on the generated output of a prediction model.

In particular, we focus on a different aspect of the problem:

Using data to identify subgroups, defined by various combinations of attributes, that experience bias due to inferior algorithm performance; illustrated in Fig. 1.

At a higher level, this problem may be connected to the concept of identifying “fairness gerrymandering,”¹⁴ where a classifier’s results are deemed “fair” for each specific group (such as race, gender, insurance status, etc.), but significantly violate fairness when it comes to structured subgroups, such as specific combinations of protected features.

Although there is prior research on this subject, our problem is unique in that we want to pinpoint specific subgroups that experience bias as a result of model performance. While the topic of identifying biased subgroups has been explored using a data mining approach (Frequent Pattern (FP) Growth algorithm)¹⁵, we present a statistically rigorous approach which directly identifies existing biased subgroups through the effective partitioning of the feature space.

Contribution.

In this this paper, we addresses the challenge of identifying bias in medical-AI models. In particular, we present a novel application of a well-studied statistical approach, specifically the Classification and Regression Trees (CART) decision trees to detect regions of bias generated by a medical-AI model, as well as the set of features that contribute to this bias. We propose an approach that identifies areas in a prediction model where patient outcomes are suboptimal. This approach allows researchers and clinicians to evaluate the reliability of a prediction model, \mathcal{A} , for a patient, p , considering their individual characteristics, X_p . This methodology can be used on the output of any arbitrary prediction model to evaluate the effectiveness of the model in making accurate predictions for a specific patient and to assess whether the model should be applied to that type of patient.

- We present a model-agnostic method to systematically and rigorously detect biased regions through the retrospective analysis of results generated by medical-AI prediction algorithms. This method addresses gaps in current fairness evaluation methods that often assume known biases and paves the way for safer and more trustworthy medical-AI applications.
- Empirically, we evaluate the effectiveness of our technique in recognizing biased regions by conducting case studies using both synthetic and real data. Our findings demonstrate our ability to identify biased regions and gain insights into the characteristics that define these regions.

2 Background

Generally, we can classify fairness into two primary categories: *individual* and *group*. Individual fairness asserts that a model should similarly treat similar people, regardless of their membership in any demographic or protected class, such as race, gender, age, and so on. Group fairness, in contrast, pertains to the concept that model results should be fair and unbiased towards selected subgroups within the population. These groupings are usually characterized by protected features to avoid discrimination against any specific subgroup and guarantee that the model’s predictions are fair and unbiased for all groups within. In this section, we focus our attention to group fairness and draw on the seminal works of Corbett-Davies et al.¹⁶ and Xu et al.¹⁷ to provide an overview of commonly used fairness definitions in the context of algorithmic bias.

*Demographic parity*¹⁶ evaluates the fairness of treatment between different protected groups, including those classified by race, sex, age, etc. This metric measures whether individuals in various categories achieve positive outcomes in proportion

to their representation in the population. Demographic parity can be expressed mathematically as follows: $P(d(X) = 1|Y = 0, X_p) = P(d(X) = 1)$. Here, $d(X) = 1$ represents a positive outcome in the algorithm's prediction, $Y = 0$ represents the absence of a specific condition, and X_p is a variable denoting membership in a protected group.

Anti-classification, also known as "Fairness Through Unawareness"¹⁸, prohibits the use of any protected features in the decision-making procedure of an algorithm. The objective is to proactively avoid any type of bias that may occur if these features were considered during the algorithm's prediction process. Although direct, this method has drawbacks when non-protected features are strongly correlated with protected features. In such cases, simply eliminating these attributes may not be sufficient to eliminate bias.

*Disparate impact*¹⁹ measures the proportion of positive outcomes for one group to the proportion for another and is often applied in legal and regulatory contexts. This metric plays an important role in identifying unintentional discrimination by analyzing the proportionality of positive outcomes between various protected attributes.

In a given dataset $\mathcal{D} = (X, Y, C)$ where X represents the protected attribute, Y includes the remaining attributes, and C is the binary class predicted by the algorithm to be predicted, disparate impact focuses on the comparisons of outcomes between different groups. It is commonly linked to the "80% rule," a principle used to detect notable disparities in treatments or outcomes. The rule is defined mathematically as follows: D has disparate impact if

$$\frac{P(C = 1|X = 0)}{P(C = 1|X = 1)} \leq \tau.$$

Here set $\tau = 0.8$.

Here, $P(C = 1|X = 0)$ and $P(C = 1|X = 1)$ represent the conditional probabilities of obtaining a positive outcome (class "1") for the minority ($X = 0$) and majority ($X = 1$) protected groups, respectively. The threshold $\tau = 0.8$ signifies that if the ratio of these probabilities falls below 80%, the system is considered to have a disparate impact, indicating a potential unintentional bias against the minority group.

Calibration, according to Corbett-Davies and Goel¹⁶, is the process of checking whether risk scores, which are estimates of the likelihood of something happening, are the same for all protected groups. This implies that a properly calibrated model's predicted probabilities accurately represent the actual probability distributions across various groups. In turn, the outcomes should be independent of any protected attributes, given the risk score. Mathematically, calibration can be defined as follows: Given risk scores $s(x)$ as predicted by the model, calibration conditions are met when

$$P(Y = 1|s(X), X_p) = P(Y = 1|s(X)).$$

The expression $P(Y = 1|s(X), X_p)$ denotes the conditional probability of the occurrence $Y = 1$ given the risk score $s(X)$ for individuals who are part of a protected group X_p . Alternatively, $P(Y = 1|s(X))$ represents the chance of the event happening for any individual who possesses an identical risk score, regardless of their affiliation to a particular group.

Equalized odds, as described by Hardt et al.²⁰, is a metric that permits the prediction \hat{Y} to be influenced by protected characteristics, but only through the target variable Y , thus preventing the features from acting as proxies for the protected attributes. This concept differs from demographic parity and promotes the use of features that enable the direct prediction of Y .

*Equal opportunity*²⁰ is a more robust indicator of equalized probabilities, which assesses whether individuals in similar circumstances have an equal probability of achieving a favorable result. In practice, this involves ensuring that the model's positive predictions are distributed evenly among various demographic groups. This implies that the model should not exhibit a bias towards any particular group when it comes to reliably recognizing true positives.

Pan et al.²¹ propose a novel machine learning (ML) framework called the "Fairness-Aware Causal Path Decomposition" framework. This model-agnostic framework places a strong emphasis on explaining and quantifying the various causal mechanisms that contribute to overall disparities in model outcomes. This approach breaks down the decision-making process of an ML model into distinct causal paths. Each path represents a specific process by which the input variables (features) influence the model's predictions. By analyzing these paths, the framework identifies how different features and their interactions impact the fairness or bias of the model.

2.1 Fairness Measure Limitations

While the group fairness measures outlined above are widely used to identify potential algorithmic bias in ML models, they have limitations. According to research by Castelnovo et al.,²² simply excluding protected features from the decision-making process does not inherently guarantee demographic parity. Achieving demographic parity may involve using different treatment strategies for different groups in order to mitigate the impact of correlations between variables, a strategy that may be considered inequitable or counter-intuitive. Dwork et al.²³ expound on a "catalogue of evils" that highlight numerous ways the satisfaction of existing fairness definitions could prove ineffective in offering substantial fairness assurances. Kleinberg et al.²⁴ discuss the inherent challenges in satisfying both calibration and balance measures, such as those proposed by equalized odds and equal

opportunity. The incompatibility of these measures underscores the complexity of achieving fairness in algorithmic systems, particularly when multiple fairness criteria are considered simultaneously.

Medical-AI decision support systems frequently function as black-box models, oftentimes providing limited insight into the structure of their training data, if any, as well as no visibility into the parameters used in model development. Developing effective and fair prediction models in this context poses unique difficulties, such as the potential absence of patient demographic representation in the training data and, in some instances, the complete absence of demographic information. Additional challenges may include the possibility of health conditions or measurement variables being used as proxies for demographic data. Additional challenges may arise due to the potential use of health conditions or measurement variables as proxies for demographic data. This occurrence can be linked to the increased prevalence of distinct conditions among specific demographic groups, potentially influenced by genetic, environmental, or socio-economic factors. On the other hand, models that do not incorporate all extensive information and health conditions of a patient may result in an oversimplified model.

3 Data

In this section, we describe the dataset used in our real-world case study. We begin with a discussion of the sepsis definition and follow with the data pre-processing steps implemented prior to model development.

3.1 Sepsis Definition

We adopted the revised Sepsis-3 definition as proposed by Singer et al.²⁵, which defines sepsis as a life-threatening organ failure induced by a dysregulated host response to infection. We implement the suspicion of infection criteria by identifying instances where the delivery of antibiotics in conjunction with orders for bacterial blood cultures occurred within a predetermined period. It is then determined that organ dysfunction has occurred when there is at least a two-point increase in the Sequential Organ Failure Assessment (SOFA) score during a specified period of time. The SOFA score is a numerical representation of the degradation of six organ systems (respiratory, coagulatory, liver, cardiovascular, renal, and neurologic)²⁶. This definition was utilized to identify patients meeting the sepsis criteria and to ascertain the most likely onset time of sepsis.

3.2 Data pre-processing

Electronic health record (EHR) data was collected from 73,484 adult patients admitted to the intensive care unit (ICU) at Grady Memorial Hospital in Atlanta, Georgia from 2016 - 2020. This data included a total of 119,733 individual patient visits, referred to as “encounters”, where, 18,464 (15.42%) visits resulted in the retrospective diagnosis of sepsis. For our study, we excluded patients with less than 24 hours of continuous data, as well as, patients diagnosed with sepsis within the first six hours, reducing our dataset to 10,274 patient encounters involving 9,827 unique patients. Among these, 1,770 (17.23%) visits were retrospectively diagnosed with sepsis during their ICU stay. The general demographic and clinical characteristics of the analyzed cohort of patients are summarized in Table 1.

The dataset includes a diverse range of continuous physiological measurements, vital signs, laboratory results, and medical treatment information for each encounter. Data also incorporated patient demographic information, including age, sex, race, zip code, and insurance status, which we utilize in later stages of the study. We performed feature reduction by removing physiological features missing more than 75% of their records. This resulted in 39 continuous patient features remaining for analysis as denoted by Table 2. Additionally, we included two administrative identifiers: procedure and ventilation status.

We impute missing data through a forward-filling approach. When a feature x has a previously recorded value, v , at time step $t_p < t$, we set $x_v^{(t)} = x_v^{t_p}$ to forward-fill the missing value of v at time step t . If no prior recorded value exists, the missing value remains unprocessed. Lastly, to mitigate data leakage, we remove sepsis patient data following their first retrospectively identified sepsis hour.

3.3 Feature engineering

Following our initial data pre-processing, which resulted in 41 selected physiological patient features, we further develop three categories of variables in this section. These include 72 variables for indicating the informativeness of missing features, 89 time-series based features, and eight clinically relevant features for assessing sepsis. The final dataset, following all feature engineering steps, resulted in a total of 210 features.

Feature informative missingness

The presence of missing data, a common occurrence in routinely collected health information, can provide significant insights, as the nature of the missing data itself can be informative²⁷. The collection times for clinical laboratory and treatment information fluctuate among individuals and may vary throughout their treatment period, resulting in a significant number of missing entries in the physiological data, including instances where entire features are absent. This phenomenon of missing data, particularly prevalent in ICU settings, is not without pattern as it often reflects the clinical judgments made regarding a patient’s

Table 1. Baseline characteristics of study patients grouped by cohort.

Variable	Overall	Grouped by sepsis			
		Non-Sepsis	Sepsis	P-Value	
n	10274	8504	1770		
Age, median [Q1,Q3]	53.0 [36.0,65.0]	53.0 [36.0,64.0]	54.0 [36.0,66.0]	0.248	
Gender, n (%)	Female	3429 (33.4)	2909 (34.2)	520 (29.4)	<0.001
	Male	6845 (66.6)	5595 (65.8)	1250 (70.6)	
Race, n (%)	Asian	125 (1.2)	99 (1.2)	26 (1.5)	<0.001
	Black	6711 (65.3)	5631 (66.2)	1080 (61.0)	
	Hispanic	479 (4.7)	387 (4.6)	92 (5.2)	
	Other	305 (3.0)	233 (2.7)	72 (4.1)	
	White	2654 (25.8)	2154 (25.3)	500 (28.2)	
ICU Length of stay (LOS), mean (SD)	6.8 (9.4)	4.3 (3.5)	19.1 (16.5)	<0.001	
No. days on ventilator, mean (SD)	3.1 (8.0)	1.0 (2.6)	13.5 (14.6)	<0.001	
LOS in hospital, mean (SD)	14.7 (19.7)	10.5 (10.5)	34.7 (35.2)	<0.001	
Albumin, mean (SD)	3.2 (0.5)	3.3 (0.5)	2.8 (0.5)	<0.001	
Anion Gap, mean (SD)	8.6 (2.3)	8.6 (2.3)	8.4 (2.2)	<0.001	
Mean Arterial Pressure (MAP), mean (SD)	93.1 (13.4)	93.4 (12.2)	91.4 (17.9)	<0.001	
Bicarbonate (HCO ₃), mean (SD)	25.7 (3.1)	25.7 (3.0)	25.3 (3.1)	<0.001	
Blood Urea Nitrogen, mean (SD)	17.7 (13.0)	16.8 (12.5)	22.2 (14.1)	<0.001	
Calcium, mean (SD)	8.3 (0.7)	8.4 (0.6)	7.9 (0.7)	<0.001	
Chloride, mean (SD)	104.6 (5.2)	104.0 (4.8)	107.9 (5.9)	<0.001	
Creatinine, mean (SD)	1.2 (1.4)	1.2 (1.5)	1.4 (1.3)	<0.001	
Weight (lbs), mean (SD)	184.2 (50.3)	182.8 (48.7)	190.8 (57.0)	<0.001	
Glasgow Comma Scale, mean (SD)	13.1 (3.1)	13.8 (2.6)	9.9 (3.5)	<0.001	
Glucose, mean (SD)	129.2 (35.0)	127.2 (35.0)	138.8 (33.1)	<0.001	
Hematocrit, mean (SD)	33.4 (6.3)	33.8 (6.4)	31.2 (5.3)	<0.001	
Hemoglobin, mean (SD)	11.2 (2.1)	11.3 (2.1)	10.6 (1.8)	<0.001	
Platelets, mean (SD)	203.9 (82.4)	208.6 (83.4)	181.6 (73.7)	<0.001	
Potassium, mean (SD)	4.0 (0.3)	4.0 (0.3)	4.0 (0.4)	0.169	
procedure, mean (SD)	0.0 (0.0)	0.0 (0.0)	0.0 (0.0)	<0.001	
Heart Rate, mean (SD)	86.2 (15.0)	85.0 (14.7)	91.8 (14.9)	<0.001	
Sodium, mean (SD)	138.8 (4.4)	138.3 (3.9)	141.6 (5.3)	<0.001	
SpO ₂ , mean (SD)	97.2 (1.8)	97.1 (1.8)	97.3 (2.0)	0.001	
Respiratory Rate, mean (SD)	18.6 (2.6)	18.4 (2.4)	19.5 (3.0)	<0.001	
White Blood Cell Count, mean (SD)	10.1 (4.3)	9.8 (4.2)	11.4 (4.7)	<0.001	
Temperature, mean (SD)	98.5 (0.9)	98.4 (0.8)	99.3 (1.1)	<0.001	

Table 2. Patient physiologic features selected for analysis

Vitals (8)	Labs (31)	
Best Mean Arterial Pressure (MAP)	Alanine Aminotransferase	Hematocrit
Heart Rate (HR)	Albumin	Hemoglobin
Oxygen Saturation (SpO ₂)	Alkaline Phosphatase	Magnesium
Respiratory Rate	Anion Gap	Partial Pressure of Carbon Dioxide (PaCO ₂)
Temperature	Aspartate Aminotransferase (AST)	Partial Pressure of Oxygen (PaO ₂)
Systolic Blood Pressure (Cuff)	Base Excess	Partial Pressure of Oxygen/Fraction of Blood Oxygen Saturation (p/F Ratio)
Diastolic Blood Pressure (Cuff)	Bicarb (HCO ₃)	pH
Mean Arterial Pressure (Cuff)	Bilirubin Total	Phosphorus
	Blood Urea Nitrogen (BUN)	Platelets
	Calcium	Potassium
	Chloride	Protein
	Creatinine	Sodium
	Daily Weight kg	White Blood Cell Count
	FiO ₂	SOFA Score Total
	Glasgow Coma Score (total)	SIRS Score Total
	Glucose	

critical condition. We introduce two missing data indicator sequences for 36 specific variables, which include all lab values, ventilation status, systolic blood pressure, diastolic blood pressure, and mean arterial pressure, with the aim to harness the latent predictive value embedded within these missing data points. The *Measurement Frequency* (f1) sequence counts the number of measurements taken for a variable before the current time. The *Measurement Time Interval* (f2) sequence records the time interval from the most recent measurement to the current time. A value of -1 is assigned when there is no prior recorded measurement.

Table 3 illustrates the application of two missing data indicator sequences through an example of an eight-hour time series for temperature measurements. The first row displays the temperature readings over time. The second row shows the measurement frequency sequence, indicating the cumulative number of temperature measurements taken up to each point in time. The final row presents the measurement time interval sequence, highlighting the time elapsed since the last temperature measurement, with a notation of -1 when there is no previous measurement to reference.

Table 3. Example of feature informative missingness sequences

	nan	98.0	98.1	nan	nan	98.2	nan	97.4
f1	0	1	2	2	2	3	3	4
f2	-1	0	0	1	2	0	1	0

Clinical empiric features

Historically, rule-based severity scoring systems for diseases like the Sequential Organ Failure Assessment (SOFA)²⁸, quick-SOFA (qSOFA)²⁵, and the National Early Warning System (NEWS)²⁹ have been used to define sepsis in clinical settings. However, these systems may not satisfy the critical need for timely detection of sepsis to initiate effective treatment³⁰. We highlight the importance of several measurements to quantify abnormalities according to some scoring system. The qSOFA score is identified as “1” with Systolic BP (SBP) ≤ 100 mm Hg and Respiration rate (Resp) ≥ 22 /min, otherwise “0”. The measurements of platelets, bilirubin, mean arterial pressure (MAP), and creatinine are scored respectively under the rules of SOFA score, while heart rate, temperature, and respiration rate are scored on the basis of the NEWS score.

Time series features

To capture the dynamic changes in patients’ data records, we calculate two types of time-series features as follows.

- *Differential features*: These are derived by computing the difference between the current value and the previous measurement of a given feature. This calculation highlights the immediate changes in patient conditions.
- *Sliding-window-based statistical features*: For this analysis, we focus on eight vital sign measurements: Best Mean Arterial Pressure (MAP), Heart Rate (HR), Oxygen Saturation (SpO2), Respiratory Rate, Temperature, Diastolic Blood Pressure (DBP), Systolic Blood Pressure (SBP), and Mean Arterial Pressure (MAP). We employ a fixed-length rolling six-hour sliding window to segment each record. This fixed rolling window increments in one-hour steps. In instances where the window is less than six hours, the sliding window includes all available data. Finally, we calculate key statistical features for each window, including maximum, minimum, mean, median, standard deviation, and differential standard deviation for each of the selected measurements.

Sepsis label lead time

This study aims to develop a prognostic model that can accurately predict the onset of sepsis up to six hours before it happens. To highlight the significance of identifying sepsis at an early stage, we have introduced a six-hour lead time on the sepsis indicator variable. This adjustment enables the model to specifically focus on and recognize probable sepsis cases before they completely develop, thereby improving the model’s ability to forecast outcomes in clinical settings.

4 Tree-based Method for Bias Detection

Given a pre-trained prediction algorithm \mathcal{A} , our objective is to identify a region \mathcal{S} in the p -dimensional feature space where the algorithm exhibits suboptimal performance, which we refer to as the “algorithmic bias” region. Here, p represents the number of features, which can be categorical and/or continuous-valued.

We assume that the true region \mathcal{S} is defined by a subset of key variables (features) $j \in S$. For real-valued features, this is represented as $X_j \in [L_j, U_j]$, where L_j and U_j represent some lower and upper bounds, respectively. For categorical value features, $X_j \in C_j$, $j \in S$. For example, if $p = 10$ and $S = \{1, 3\}$, the algorithmic bias region might be defined by age $X_1 \in [35, 50]$ and gender $X_3 = \{\text{Female}\}$.

This formulation implies that the subset of variables in the set S will be the most critical in causing the bias, defining the algorithmic bias region \mathcal{S} . For instance, in our example, age and gender are the two most important features in defining the algorithmic bias region \mathcal{S} . Fig. 2 illustrates the idea, where the algorithmic bias region is a box in the feature space for $X \in \mathbb{R}^p$.

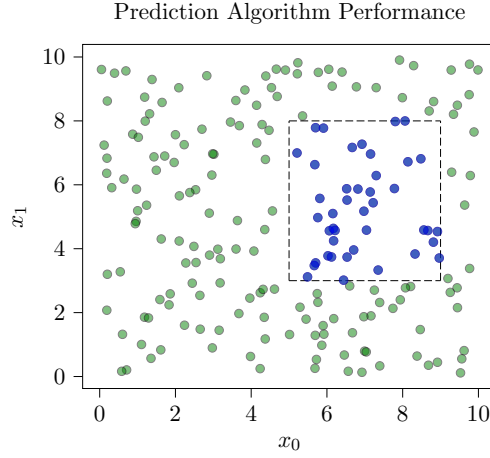


Figure 2. Illustration of the algorithmic bias region \mathcal{S} in the feature space, where the algorithm \mathcal{A} exhibits suboptimal performance.

Without knowing the true algorithmic bias region, \mathcal{S} , of the algorithm \mathcal{A} , as represented using blue dots in Fig. 2, we want to estimate it using test data. We can evaluate the performance of the algorithm on a collection of test samples $x_i \in \mathbb{R}^p$, $i = 1, \dots, n$. The response associated with each test sample is $y_i \in \mathbb{R}$. Based on this, we can evaluate the algorithm performance using residuals.

$$\varepsilon_i = y_i - f(x_i), \quad i = 1, \dots, n.$$

We note that alternative measures of algorithm performance, such as conformity scores, may replace residuals.

Our goal is to estimate the region $\widehat{\mathcal{S}}$ using $\{\varepsilon_i\}_{i=1}^n$ as follows:

$$\widehat{\mathcal{S}} = \{X_j \in [L_j, U_j] \text{ or } X_j \in C_j, j \in \widehat{S}\}, \tag{1}$$

where S , L_j , U_j , and C_j are parameters to be determined. Continuing with our previous example, if we estimate $\widehat{S} = \{1, 5\}$, this implies that we have correctly predicted the first important feature and incorrectly predicted the second. If $\widehat{S} = S$, then we estimate the correct subset variables used to define the algorithmic bias region. Once S is estimated, the other parameters can be easier to decide.

We hypothesize that the residuals within the bias region are larger. Thus, we formulate our problem as follows.

$$\max_{\widehat{S}} \frac{1}{n(\widehat{S})} \sum_{x_i \in \widehat{S}} |\varepsilon_i|, \tag{2}$$

where \widehat{S} is defined in (1), and $n(\widehat{S})$ represents the number of data points \widehat{S} .

We apply decision trees, specifically Classification And Regression Trees (CART), as proposed by Breiman et al.³¹, to solve (2) with a regularization term accounting for tree complexity. The CART algorithm recursively partitions the feature space until some stopping criteria is achieved and provides a piecewise-constant approximation of the response function, here representing algorithm performance. The effectiveness of our methodology relies on the compactness of the estimated value \widehat{S} to the true value S . This distance measure will be assessed using test samples (x_i, y_i) , taking into account the inherent stochastic nature of the data. This bias detection method serves to audit the performance of any given pre-trained prediction algorithm \mathcal{A} and is thus model agnostic as represented in Fig. 1.

4.1 Classification and Regression Trees (CART)

Decision trees are a versatile and intuitive machine learning (ML) algorithm used for both classification and regression tasks, embodying a tree-link model of decisions and their possible consequences. The CART model³¹, is a non-parametric ML

decision tree methodology that is well suited for the prediction of dependent variables through the utilization of both categorical and continuous predictors. CART models offer a versatile approach to defining the conditional distribution of a response variable y based on a set of predictor values x ³².

In the classification setting, we are given the training data (\mathbf{X}, \mathbf{Y}) , containing n observations (\mathbf{x}_i, y_i) , $i = 1, \dots, n$, each with p features $\mathbf{x}_i \in \mathbb{R}^p$ and a class label $y_i \in \{1, \dots, K\}$ indicating which of K possible labels is assigned to this given point. In the regression setting our output variable is a continuous response variable $y_i \in \mathbb{R}$. Decision tree methods seek to recursively partition the dataset (feature space) into a number of hierarchically disjoint subsets with the aim of achieving progressively more homogeneous distributions of the response variable y within each subset. An example of a decision tree is shown in Fig. 3.

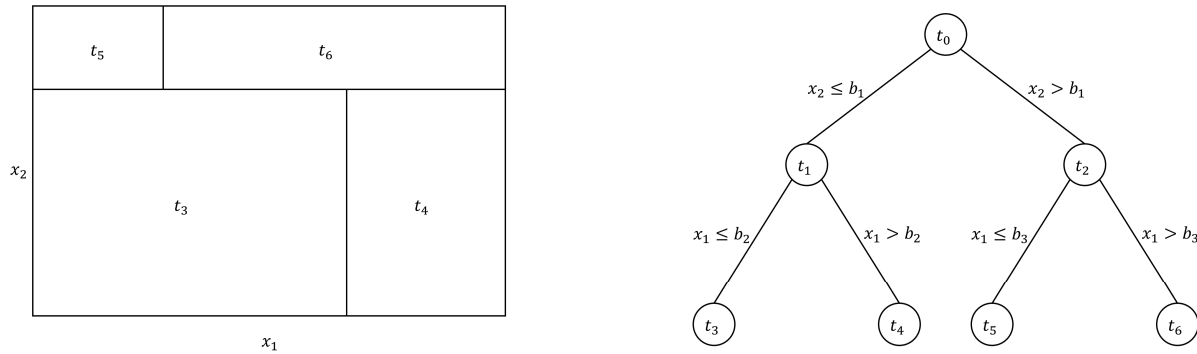


Figure 3. Example of an optimal axis-aligned decision tree with a depth of $K = 2$ with $p = 2$ dimensions. Splits occur along specific features in the form $x_j = b$ for $j = 1, 2$.

Beginning from the root node, an optimal feature and split point are identified based on an appropriate optimization metric. The feature, split-point pair defines the partition splitting the feature space, and this procedure is repeated for every sub-feature space that is created. These partitions will ultimately result in the binary tree structure consisting of interconnected root, branch, and leaf nodes.

- *Root* nodes encapsulate the entire dataset, forming the foundational layer of the decision tree.
- *Branch* nodes are points in the dataset characterized by features and split points that serve as points of division for partitioning the feature space. Each of these branches extend to subsequent child nodes.
- *Leaf* nodes are the final nodes in the tree, classifying or predicting data points based on their localized patterns.

CART models take a top-down approach and can be used for both classification and regression problems, as the name implies. Partitions are determined by using a specified loss function to evaluate the quality of a potential split and are based on both the features and values, that provide optimal splits. The splitting criteria determine the optimal splits. In the classification setting, the criteria are often determined by the label impurity of data points within a partition. The splitting criteria for regression-based CART models focuses on minimizing the variance of data points in partitioned regions. CART models, as applied to both tasks, have two main stages: the decision tree’s generation and subsequent pruning. We now transition to a more granular discussion on CART’s implementation for both classification and regression problems.

Classification Trees

The CART method, in the context of classification tasks, is a powerful tool for categorizing outcomes into distinct classes based on input features. The objective is to partition the feature space into regions that maximize the the uniformity of the response variable’s classes within in each subsequent node during the partitioning process. This process begins at the root node and splits the feature space recursively based on a set of decision rules that maximally separate the classes.

When we consider splitting a classification tree, T , at any node t , we evaluate potential splits based on how well they separate the different classes of the response variable. For a given variable X , a split point s is chosen to divide node t into left (t_L) and right (t_R) child nodes. This division is based on whether the values of X are less than or equal to s or greater than s , formally defined as $t_L = \{\mathbf{X} \in t : X \leq s\}$ and $t_R = \{\mathbf{X} \in t : X > s\}$. The effectiveness of a split is measured using the impurity metric of Information Gain, which gauges the value of the insight a feature offers about a response variable. In practical applications, this measure is determined using Entropy or the Gini index.

- *Entropy* functions as a metric of disorder or unpredictability. It measures the impurity or randomness of a node, especially in binary classification problems. Mathematically, it is expressed as:

$$E = - \sum_{i=1}^K p_i \log_2 p_i,$$

where p_i is the probability of an instance belonging to the i^{th} class.

- *Gini index* serves as an alternate measure of node impurity. Considered a computationally efficient alternative to entropy, it is formulated as follows:

$$E = \sum_{i=1}^K p_i(1 - p_i),$$

where, yet again, p_i is the probability of an instance belonging to the i^{th} class.

- *Information Gain* is a metric calculated by observing the impurity of a node before and after a split and is formulated as:

$$\text{IG} = E_{\text{parent}} - \sum_{i=1}^K w_i E_{\text{child}_i},$$

where w_i is the relative weight of the child node with respect to the parent node.

The algorithm uses these splitting criteria to divide the feature space into sub-regions recursively, terminating when any of the specified stopping criteria are satisfied. After the dividing procedure finishes, each region gets assigned a class label $1, \dots, K$. This assigned class label will predict the classification of any points inside the region. Typically, the assigned class will be the most common class among the points in the region.

Regression Trees

Regression trees exhibit notable performance in the prediction of continuous output variables. The key aspect of their approach involves partitioning the feature space in such a way that the variation of the target variable is minimized within each segment of the space, referred to as nodes. To elaborate, when a regression tree, denoted as T , undergoes a split at a node t , we consider a potential division point, or split point s , for a variable X . This split point categorizes the data into left (t_L) and right (t_R) child nodes based on the condition whether $X \leq s$ or $X > s$. These nodes are formally represented as $t_L = \{\mathbf{X} \in t : X \leq s\}$ and $t_R = \{\mathbf{X} \in t : X > s\}$. The criterion for assessing the quality of a split in regression trees revolves around the variance within a node, given by

$$\widehat{\Delta}(t) = \widehat{\text{VAR}}(y|\mathbf{X} \in t) = \frac{1}{n(t)} \sum_{\mathbf{x}_i \in t} (y_i - \bar{y}_t)^2,$$

where \bar{y}_t is the mean value of the target variable for the data points within node t and $n(t)$ represents the count of these data points. The variance within the child nodes, left (t_L) and right (t_R), is similarly calculated. The decision to split a parent node t into child nodes is based on the split that yields the highest decrease in variance, defined as

$$\widehat{\Delta}(s, t) = \widehat{\Delta}(t) - (\widehat{W}(t_L)\widehat{\Delta}(t_L) + (\widehat{W}(t_R)\widehat{\Delta}(t_R)),$$

where $\widehat{W}(t_L) = n(t_L)/n(t)$ and $\widehat{W}(t_R) = n(t_R)/n(t)$ denote the proportions of data points in t allocated to t_L and t_R , respectively.

The process of developing the tree T is iterative, identifying the variable and split point that maximizes variance reduction. Similar to its classification counterpart, the recursive partitioning of the feature space aims at reducing variance with the ultimate goal of accurately estimating the conditional mean response $\mu(x)$, in the tree's terminal nodes. The predicted response for data points in node t is the mean target variable value, \bar{y}_t , for those points.

Tree Pruning

Without limitations, the tree generation process of the CART algorithm will continue until each data point is represented by a single leaf node. This is often not recommended as fully growing a tree to maturity introduces the risk of overfitting. To counter this, the tree development process includes constraints such as minimal sample split, maximum tree depth, and cost-complexity pruning to fine-tune the tree's structure and fit. Another procedure to reduce tree complexity is via the introduction of a complexity regularization technique that mitigates the effects of poor generalization on unseen data that may be introduced by

overfitting. Cost-complexity pruning, also known as weakest link pruning, involves the selective removal of branches, that contribute least to prediction accuracy, from the tree to promote improved generalization. The pruning process works upwards through the partition nodes from the bottom of the tree. In particular, it uses a parameter α to strike a balance between the depth of a decision tree and its fit to the training data. The trade-off is quantified by

$$R_\alpha(T) = R(T) + \alpha|T|,$$

where $R(T)$ is the misclassification rate of the tree T and $|T|$ represents the count of the terminal nodes. The parameter $\alpha \geq 0$ controls the trade-off, with larger values of α resulting in smaller trees.

5 Sepsis Prediction Model

In developing the sepsis prediction model, we reference the model development procedure described in Yang et al.³³, which is one of the best-performing algorithms for sepsis detection. This section begins with an overview of the XGBoost model that was created for the sepsis prediction task. Next, we detail the data partitioning process by which we generated the training, validation, and test sets. Finally, we assess the model's performance.

5.1 XGBoost Model

The sepsis prediction model developed for this analysis was centered on the implementation of XGBoost³⁴, a robust tree-based gradient boosting algorithm known for its high computational efficiency and exceptional performance in managing complex and large datasets. We constructed this model using the Bayesian optimization technique with a Tree-structured Parzen Estimator (TPE)³⁵ approach. We applied this method to optimize hyperparameters, which helped establish the learning process, complexity, and generalization capability of the model. Hyperparameters included but were not limited to, the following: max depth, learning rate, and alpha and lambda regularization terms.

The Bayesian optimization technique involved a series of 20 evaluations. In each iteration, we tune the hyperparameters with the aim of maximizing the accuracy of the prediction model. The final model is an ensemble based on the average five-fold cross-validation performance measured across this accuracy optimized loss function.

5.2 Training, validation, and test sets

In crafting our machine learning model, we incorporated a nuanced approach that integrates stratified cross-validation, temporal partitioning of data, and ensemble techniques to address the inherent challenges of predicting sepsis through use of temporal dataset. This framework is specifically designed to evaluate models on future, unobserved data, thus closely simulating real-world clinical forecasting scenarios and enhancing the model's external validity. Our stratification strategy ensures that each subset for training and validation is a representative sample of the entire dataset by addressing class imbalance across folds. We incorporate an ensemble methodology to leverage the collective insights from multiple models, with the aim to reduce variability and enhance the reliability across predictions.

To construct our training, validation, and testing datasets we initially divided the dataset temporally, creating two groups: one with patients admitted to the ICU prior to 2019, designated for training and validation purposes, and the other comprised of patients from 2019 onwards for testing. The training and validation set consisted of 6,364 patient encounters, with 1,195 cases of sepsis and 5,169 cases of non-sepsis sequences. Similarly, the test set consisted of 3,910 patient encounters, with 575 cases of sepsis and 3,335 cases of non-sepsis sequences. Within the pre-2019 dataset, we performed stratified five-fold cross-validation to further partition the data into five exhaustive and mutually exclusive subsets. We execute this stratification with respect to the sepsis label to guarantee that each fold contains a proportional distribution of cases, both septic and non-septic.

Within each of these five stratified folds we include all relevant continuous physiological data for each patient, reflecting the previously mentioned comprehensive feature engineering process that was undertaken. We further temporally partition this data, allocating the initial 24 hours of records following a patient's admission to the ICU to the training set, and the subsequent records, up to the 168th hour, to the validation set. This 168-hour cap is strategically selected to reduce the potential impacts of data bias that might arise from complications affecting a patient's health status beyond the initial week of their ICU stay. To address the imbalance between sepsis and non-sepsis hours, we also undertake a down sampling of the non-sepsis instances within each fold. Each fold thus generates a model trained on its designated training data subset and validated on its respective validation set. Collectively, these models form an ensemble, capitalizing on the variability and strengths of each model trained and validated on slightly different data segments. The visual representation of the complete data pre-processing and model development pipeline is depicted in Fig. 4.

5.3 Model results

Table 4 presents a horizontal comparison between the individual and ensemble models across the aforementioned prediction metrics.

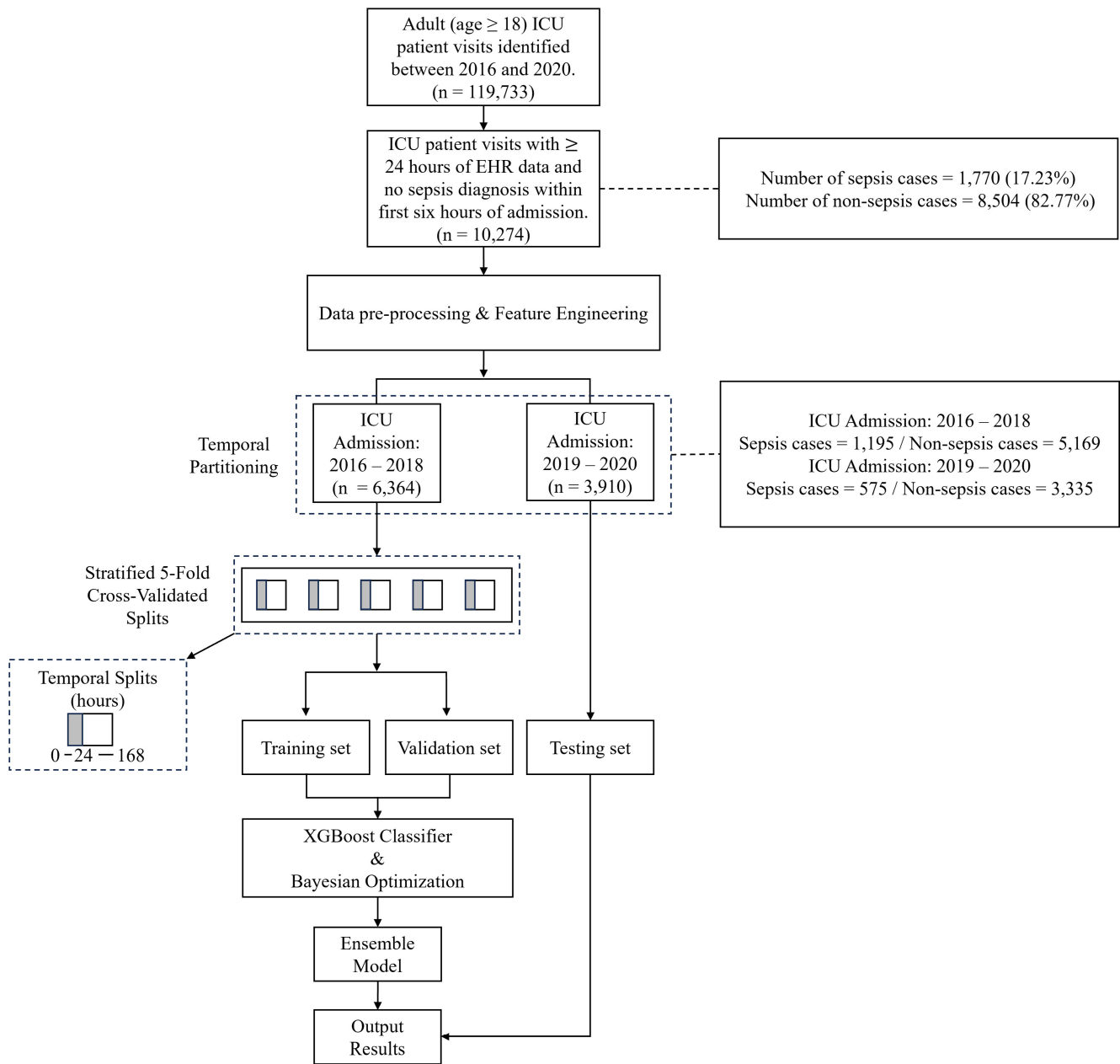


Figure 4. Illustration of the data pre-processing and model development procedure of the sepsis prediction model.

Table 4. Performance of different models on local test set formed by ourselves

XGBoost Models (Folds)	Accuracy	AUC
1	0.821	0.747
2	0.811	0.692
3	0.807	0.692
4	0.777	0.710
5	0.814	0.724
Average	0.810	0.716
Ensemble Model	0.828	0.735

We summarize the complete performance of our sepsis prediction model in Fig. 5. The results are organized according to

the two previously described phases of the analysis, with each phase focused on different subsets of data. The first row of Fig. 5 depicts the performance of the model based on the analysis of the training set. Fig. 5a illustrates the ability of the model to predict sepsis using a confusion matrix that presents the quantity (and proportion) of true positives, false positives, true negatives, and false negative results. Fig. 5b presents the receiver operator characteristics (ROC) curve. The ROC curve is a graphical representation that shows the diagnostic ability of the prediction model by displaying the true positive rate (recall) versus the false positive rate (specificity) at different threshold values. The second row of the figure examines the model's performance on unseen data, providing insight into how well the model generalizes to unseen data. Similarly to the first row, Fig. 5c illustrates the model's predictive performance through a confusion matrix, while Fig. 5d displays the ROC curve for the test data. Table 5 provides a detailed summary of the classification performance metrics of the prediction model.

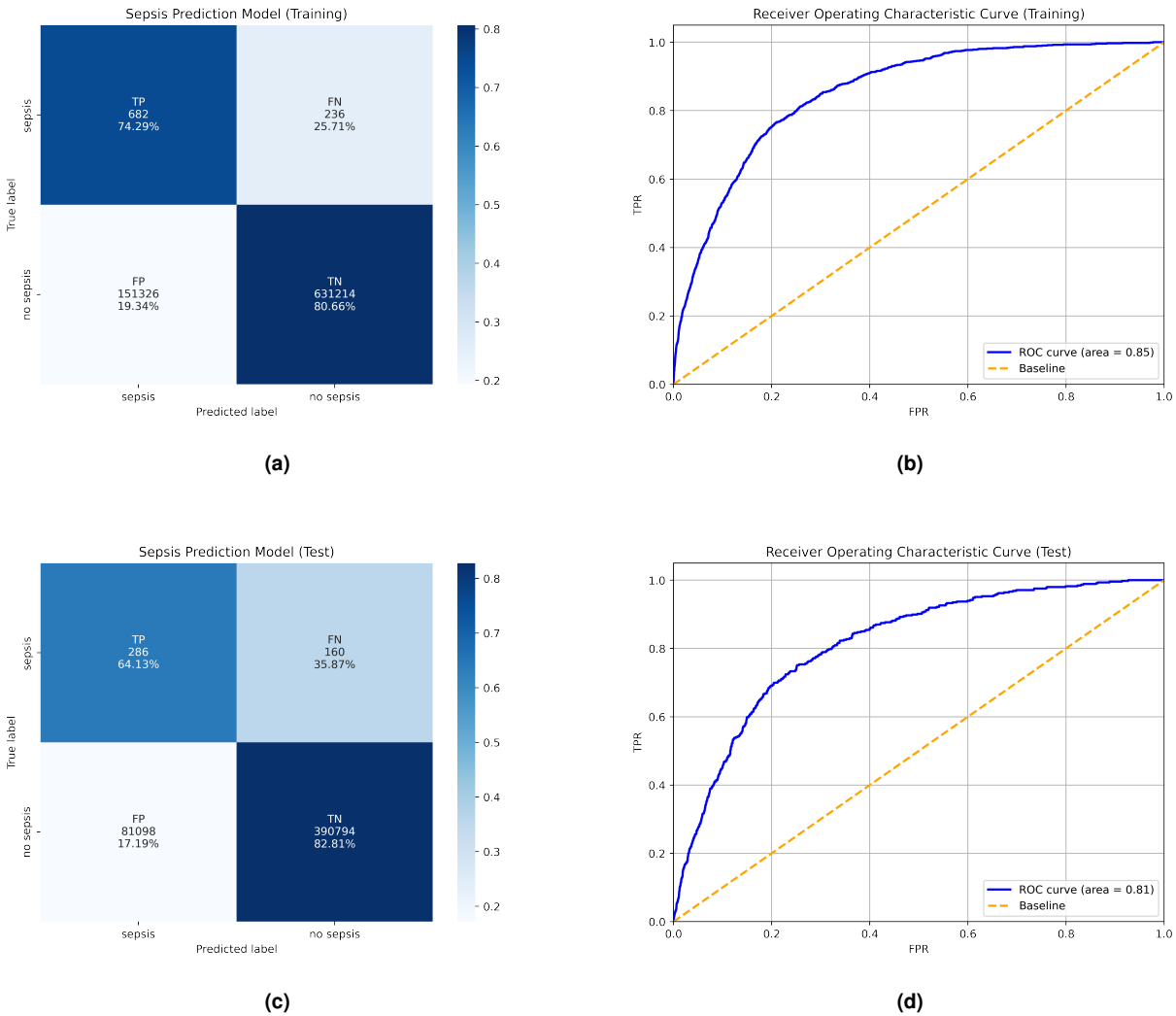


Figure 5. The plots present the sepsis prediction model's performance measures. Plots (a) and (b) show the confusion matrix and ROC curve results of the model against the training data, respectively. Plots (c) and (d) provide similar measures for the test dataset.

	Accuracy	Precision	Recall	F1-Score	F2-Score
Training Set	0.807	0.004	0.743	0.009	0.022
Test Set	0.828	0.004	0.641	0.007	0.017

Table 5. Sepsis prediction model classification performance metrics for training and test sets.

6 Synthetic Data Experiment

In this section, we conduct experiments utilizing two synthetic data simulations. The objective of the simulation studies is to methodically assess the effectiveness of the CART algorithm in the context of detecting algorithmic bias regions. This comparison is carried out by evaluating the coverage ratio, which serves as our primary performance criterion. This metric has been designed to effectively analyze and encompass the potential presence of an algorithmic bias region that may emerge within the feature space.

6.1 Performance Metrics

We introduce a refined performance metric, namely the coverage ratio, designed to account for the presence of distinct region(s) characterized by algorithmic bias within the feature space.

Coverage Ratio in n -Dimensional Space

The Coverage Ratio in n -dimensional space is a metric that quantifies the relationship between the hypervolumes of the true and estimated regions compared to the overlapping hypervolume covered by both regions. When $n = 2$ or $n = 3$, the coverage ratio is comparable to measuring the ratio of overlap between the area or volume of two sets, respectively. This metric is extended to higher-dimensional spaces as follows:

Given a dataset $\mathcal{D} \subset \mathbb{R}^n$, consider two n -dimensional bounded regions defined by sets \mathcal{S} (true region) and $\hat{\mathcal{S}}$ (estimated region). Let $|\mathcal{S} \cap \hat{\mathcal{S}}|$ denote the hypervolume of overlap common to both regions. The coverage ratio, CVR , for N regions in an n -dimensional space is defined as:

$$CVR = \frac{1}{2N} \sum_{i=1}^N \left(\frac{|\mathcal{S}_i \cap \hat{\mathcal{S}}_i|}{|\mathcal{S}_i|} + \frac{|\mathcal{S}_i \cap \hat{\mathcal{S}}_i|}{|\hat{\mathcal{S}}_i|} \right). \quad (3)$$

Here, $|\mathcal{S}_i|$ and $|\hat{\mathcal{S}}_i|$ represent the hypervolumes of the true and estimated regions, respectively, in the n -dimensional space. The Coverage Ratio provides a measure of how well the estimated region approximates the true region in higher-dimensional space.

6.2 Synthetic data

To investigate the impacts of algorithmic bias within a feature space, we generated synthetic datasets, using multidimensional uniform distributions. In this simulation, we perform a set of experiments using a single implicit bias region on a range of sample sizes. In the setting where $p \in [2, 3]$, $n_s = [500, 750, 1000, 2000, 3000, 6000, 8000]$. In the setting where $p \in [4, 5]$, $n_s = [5000, 7500, 10000, 20000, 30000, 60000, 80000]$. Features $x_i \in i = 1, 2, \dots, 5$ were selected from a uniform distribution within the restricted range of $[-10, 10]$. The corresponding y values for these data points were produced similarly from a uniform distribution, spanning the range $[0.8, 1.0]$. To incorporate algorithmic bias regions with alternate output distribution, a central point, denoted c_i , was stochastically chosen within the feature space. Subsequently, the data points located within a specified radius around the given central point were modified to ensure that their corresponding output values, y , followed a uniform distribution limited to the interval $[0.3, 0.6]$. The region having reduced output values in the feature space is indicative of the region that may possess algorithmic biases.

The focus of our initial experiment was to explore the relationship between the topology of the data samples and the resulting performance of the CART model given a fixed predefined algorithmic bias region. For each sample size, n_s , we established a single algorithmic bias region, which was maintained consistently throughout each replication of the experiment as our benchmark (true regions). The emphasis here was on experimenting with the positional variability of data points with the random generation of new data points in each replication.

In the second experiment, our objective was to measure the influence exerted by the location of the algorithmic bias region on the performance of the CART model. This experiment maintained a fixed feature space topology across each replication, allowing the analysis to focus on the implications of varying the location of the algorithmic bias region.

The effectiveness of the model was evaluated using the Coverage Ratio performance metric as described above. This metric was used to compare the estimated region produced by the model with the previously defined true region.

6.3 Results

The simulation aimed to investigate the complex relationships between algorithmic bias regions and feature space topologies. Using a systematic and rigorous methodology, the experiments sought to gain insight into how these relationships affect the performance and reliability of the CART model. Fig. 6 provides a visual representation of the ability of our approach to accurately estimate the borders of regions characterized by algorithmic bias. The true region(s) are delineated and filled in blue, whereas the estimated region(s) consist of points located inside the red dashed lines. Fig. 6a illustrates an example of the simulated output in the context of a two-dimensional scenario. Similarly, Fig. 6b demonstrates the ability to identify algorithmic biases in a three-dimensional scenario. We provide a summary of the results achieved by our approach, as depicted

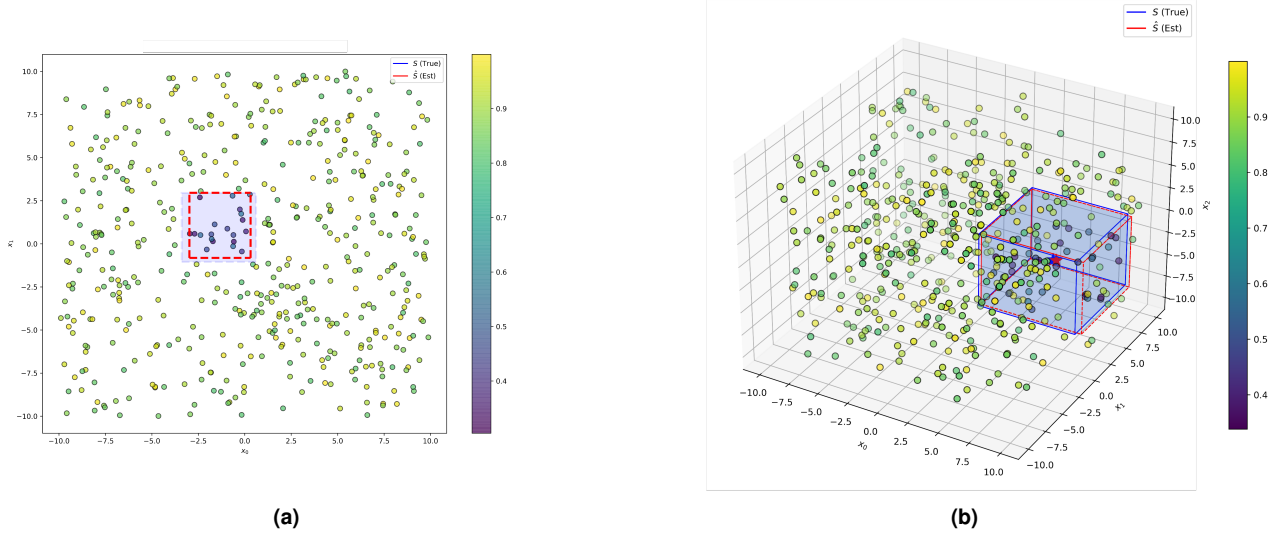


Figure 6. Examples of the experimental results in 2(a) and 3(b) dimensional space.

in Fig. 7, and confirm the efficacy of the CART algorithm in accurately detecting algorithmic bias regions. To provide precise details, Fig. 7 shows the mean performance of each experiment at the various sample size test points for multiple n -dimensional cases. The figures incorporate 95% confidence intervals for both experiments. These results indicate that our method can efficiently detect the presence of algorithmic bias layered in the feature space.

7 Real-Data Experiment

In the second phase of our empirical study, we evaluate the effectiveness of the sepsis prediction model and aim to identify any potential algorithmic biases. During this assessment, the test dataset is used to sequentially process the continuous data of each patient via the prediction model. We further refine the test data by only applying the model to patients whose EHR data includes at least one occurrence of sepsis. Implementing this approach results in an hourly forecast for every occurrence of a patient’s data. Subsequently, we compute the performance of the classification model for every individual patient. Here, we selected model accuracy as the performance measure, implying it is the variable we are using to identify algorithmic bias. Next, we combine the accuracy of each patient’s performance measure with their corresponding demographic data, which includes a range of factors such as gender, race, age, insurance type, and the existence and number of pre-existing comorbidities. One-hot encoding is used to transform non-numeric features into a numeric representation. In addition, we use a five-fold cross-validated grid search strategy to enhance the performance of the CART algorithm. This technique helps us determine the optimal selection of hyperparameters for the decision tree model. The hyper-parameter grid utilized for this investigation is denoted by Table 6.

Parameters	Grid
“criterion”	[“mse”, “absolute_error”]
“splitter”	[“best”]
“ccp_alpha”	[0.0005, 0.001, 0.01, 0.1, 0.2, 0.3, 0.4, 0.5]
“max_depth”	[3,5,7]
“min_samples_leaf”	[30,50,70,100]
“min_samples_split”	[30,60,100,150,200,300]
“max_features”	[“auto”, “log2”, “sqrt”]

Table 6. CART bias detection hyper-parameter tuning grid

7.1 Results

The final result of our bias detection model is shown in Figure 8. Branch nodes offer details on the feature split-point pair selected by the model at each split, the number of instances included in the node, and the average value of the response variable

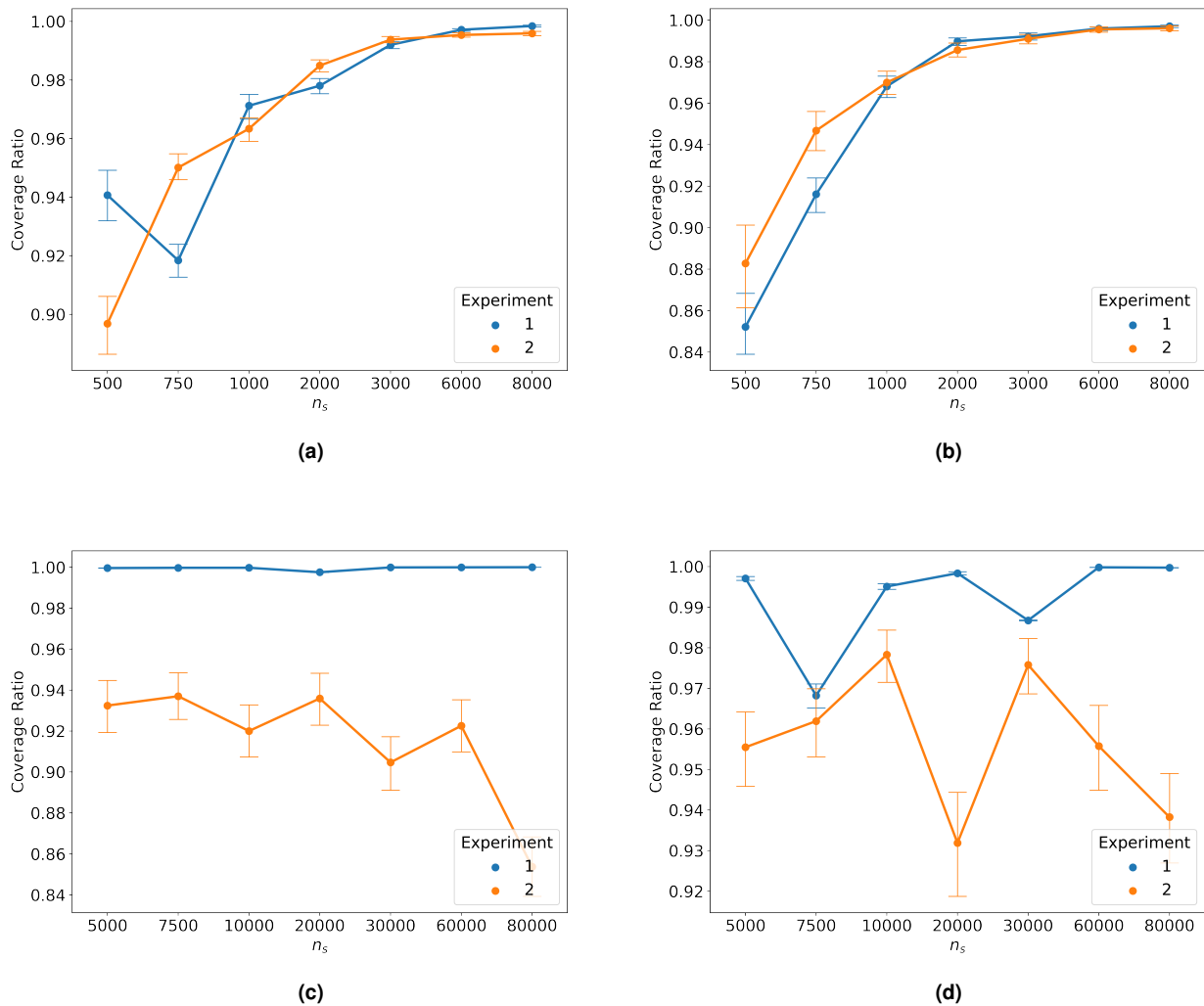
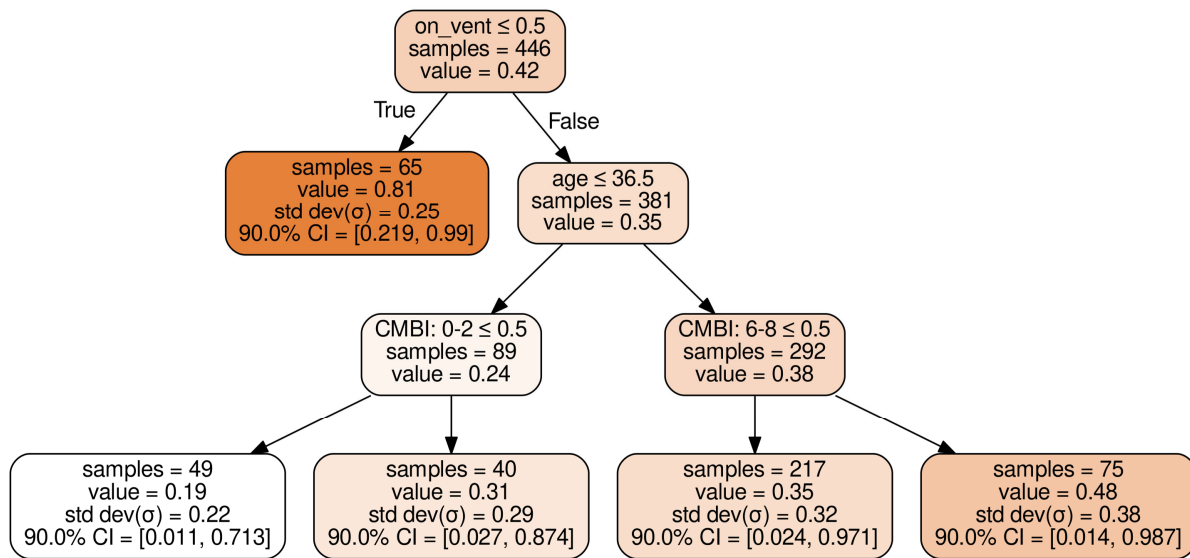


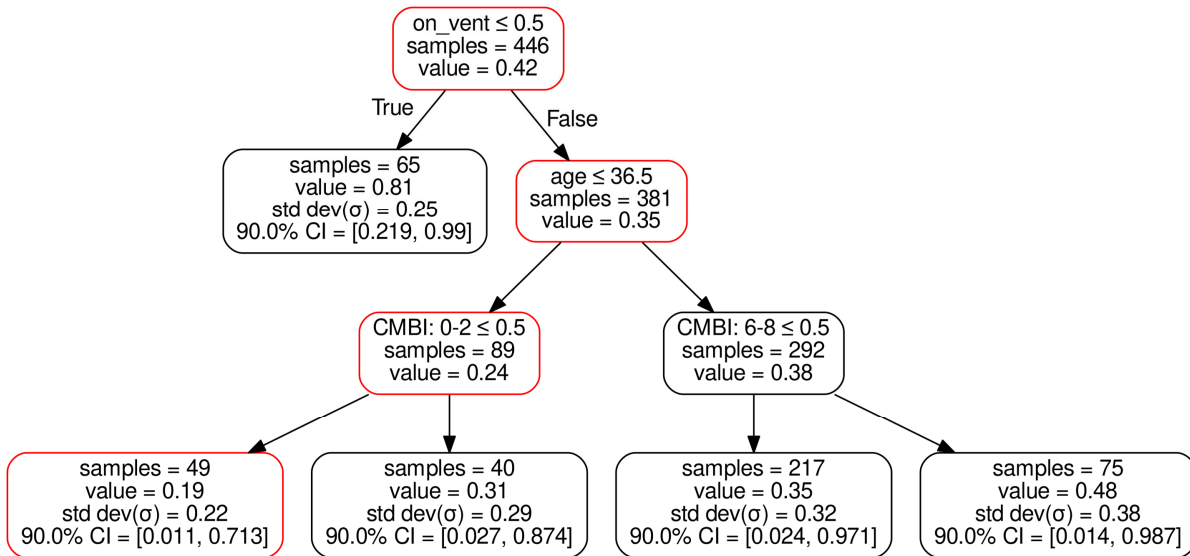
Figure 7. The plots show the mean coverage ratio for multiple n -dimensional test points: 2D(a), 3D(b), 4D(c), and 5D(d).

y for the examples inside the node. Similarly, the leaf nodes offer the count of instances inside the node. However, the values assigned to these nodes indicate the model’s point prediction \hat{y} for every data point that falls within them. Furthermore, we have included the standard deviation of the response variable in each leaf node. Additionally, we quantify the uncertainty of the point estimate prediction by providing a 90% confidence interval (CI) based on quantiles. This interval indicates the range of values containing the true performance of the model’s output for patients who meet the specified criteria, with a high level of confidence. Fig 8a illustrates the comprehensive decision tree produced by the results of the sepsis prediction model for the test data. Fig 8b highlights the leaf node which exhibits the most significant level of poor performance. The data points assigned to this node have a point prediction of 0.19, along with a 90% confidence interval of [0.011, 0.713]. The identification of this node signifies the presence of algorithmic bias within a specific region of the feature space and traces its origin back to the root node. Fig 8c illustrates a simplified representation of the attributes that make up this suboptimal route. The feature label beginning with “CMBI” reflects a discretized count of the pre-existing comorbidities, based on the Charlson Comorbidity Index (CMBI), that a patient possesses. Based on our bias detection technique, we might conclude that the given sepsis prediction model \mathcal{A} may not perform well for “Ventilated patients, younger than 37 years old, with more than 2 pre-existing conditions.” This summary provides a concise and pragmatic explanation of the course of the decision tree, enabling an improved understanding of the demographic and clinical attributes of the patient(s) associated with these areas of suboptimal performance.

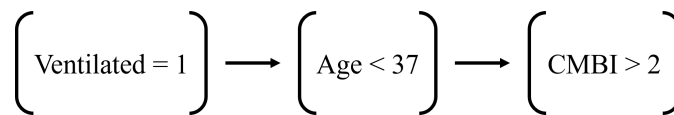
Tracing decision tree routes and evaluating them in this way offers useful information about the decision-making process of the model. It emphasizes the key variables that have the greatest impact on the model’s predictions, enabling us to identify and



(a)



(b)



(c)

Figure 8. Decision tree generated as a result of our bias detection methodology. 8(a) displays the complete decision tree, 8(b) emphasizes the path from the region exhibiting the worst suboptimal performance to the root node, and 8(c) illustrates a simplified representation of the nodes along that route.

potentially mitigate any potential biases in the model’s sepsis prediction approach.

8 Conclusion

This paper presents a new approach to detect and analyze regions of algorithmic bias in medical-AI decision support systems. This framework, which uses the Classification and Regression Trees (CART) method, is an important step in recognizing and

dealing with potential biases in AI applications in the healthcare sector. We evaluated our technique through synthetic data experiments and successfully demonstrated the method's ability to identify areas of bias, assuming that such regions exist in the data. Additionally, we extended our examination to a real-world dataset by carrying out an experiment using electronic health record (EHR) data obtained from Grady Memorial Hospital.

The increasing integration of machine learning and artificial intelligence in healthcare highlights the pressing requirement for tools, techniques, and procedures that guarantee the fair and equitable use of these technologies. The framework we present provides a tangible solution to this challenge. It offers a means for healthcare practitioners and AI developers to identify and remedy algorithmic biases, therefore promoting the development of medical ML/AI decision support systems that are both ethically sound and clinically effective.

Acknowledgement

This work is partially supported by an NSF CAREER CCF-1650913, NSF DMS-2134037, CMMI-2015787, CMMI-2112533, DMS-1938106, DMS-1830210, Emory Hospital, and the Coca-Cola Foundation.

References

1. Patel, N. M. *et al.* Enhancing Next-Generation Sequencing-Guided Cancer Care Through Cognitive Computing. *The Oncol.* **23**, DOI: [10.1634/theoncologist.2017-0170](https://doi.org/10.1634/theoncologist.2017-0170) (2018).
2. Shaheen, M. Y. Applications of Artificial Intelligence (AI) in healthcare: A review. *Sci. Prepr.* (2021).
3. Narayanan, A. Tutorial: 21 Fairness Definitions and their Politics. *Conf. on Fairness, Accountability, Transpar.* (2018).
4. Vela, M. B. *et al.* Eliminating Explicit and Implicit Biases in Health Care: Evidence and Research Needs, DOI: [10.1146/annurev-publhealth-052620-103528](https://doi.org/10.1146/annurev-publhealth-052620-103528) (2022).
5. Blair, I. V., Steiner, J. F. & Havranek, E. P. Unconscious (Implicit) Bias and Health Disparities: Where Do We Go from Here? *The Perm. J.* **15**, DOI: [10.7812/tpp/11.979](https://doi.org/10.7812/tpp/11.979) (2011).
6. Fitzgerald, C. & Hurst, S. Implicit bias in healthcare professionals: A systematic review. *BMC Med. Ethics* **18**, DOI: [10.1186/s12910-017-0179-8](https://doi.org/10.1186/s12910-017-0179-8) (2017).
7. Hall, W. J. *et al.* Implicit racial/ethnic bias among health care professionals and its influence on health care outcomes: A systematic review, DOI: [10.2105/AJPH.2015.302903](https://doi.org/10.2105/AJPH.2015.302903) (2015).
8. Greenwald, A. G. *et al.* Implicit-Bias Remedies: Treating Discriminatory Bias as a Public-Health Problem. *Psychol. Sci. Public Interest* **23**, DOI: [10.1177/15291006211070781](https://doi.org/10.1177/15291006211070781) (2022).
9. Obermeyer, Z., Powers, B., Vogeli, C. & Mullainathan, S. Dissecting racial bias in an algorithm used to manage the health of populations. *Science* **366**, DOI: [10.1126/science.aax2342](https://doi.org/10.1126/science.aax2342) (2019).
10. Pencina, M. J., Goldstein, B. A. & D'Agostino, R. B. Prediction Models — Development, Evaluation, and Clinical Application. *New Engl. J. Medicine* **382**, DOI: [10.1056/nejmp2000589](https://doi.org/10.1056/nejmp2000589) (2020).
11. Larson, J., Mattu, S., Kirchner, L. & Angwin, J. How We Analyzed the COMPAS Recidivism Algorithm. *ProPublica* (2016).
12. Larrazabal, A. J., Nieto, N., Peterson, V., Milone, D. H. & Ferrante, E. Gender imbalance in medical imaging datasets produces biased classifiers for computer-aided diagnosis. *Proc. Natl. Acad. Sci. United States Am.* **117**, DOI: [10.1073/pnas.1919012117](https://doi.org/10.1073/pnas.1919012117) (2020).
13. Gianfrancesco, M. A., Tamang, S., Yazdany, J. & Schmajuk, G. Potential Biases in Machine Learning Algorithms Using Electronic Health Record Data, DOI: [10.1001/jamainternmed.2018.3763](https://doi.org/10.1001/jamainternmed.2018.3763) (2018).
14. Kearns, M., Neel, S., Roth, A. & Wu, Z. S. Preventing fairness gerrymandering: Auditing and learning for subgroup fairness. In *35th International Conference on Machine Learning, ICML 2018*, vol. 6 (2018).
15. Pastor, E., de Alfaro, L. & Baralis, E. Identifying Biased Subgroups in Ranking and Classification. In *Responsible AI @ KDD 2021 Work.* (2021).
16. Corbett-Davies, S. & Goel, S. The Measure and Mismeasure of Fairness: A Critical Review of Fair Machine Learning. *J. Mach. Learn. Res.* **24** (2023).
17. Xu, J. *et al.* Algorithmic fairness in computational medicine, DOI: [10.1016/j.ebiom.2022.104250](https://doi.org/10.1016/j.ebiom.2022.104250) (2022).
18. Kusner, M., Loftus, J., Russell, C. & Silva, R. Counterfactual fairness. In *Advances in Neural Information Processing Systems*, vol. 2017-December (2017).

19. Feldman, M., Friedler, S. A., Moeller, J., Scheidegger, C. & Venkatasubramanian, S. Certifying and removing disparate impact. In *Proceedings of the ACM SIGKDD International Conference on Knowledge Discovery and Data Mining*, vol. 2015-August, DOI: [10.1145/2783258.2783311](https://doi.org/10.1145/2783258.2783311) (2015).
20. Hardt, M., Price, E. & Srebro, N. Equality of opportunity in supervised learning. In *Advances in Neural Information Processing Systems* (2016).
21. Pan, W., Cui, S., Bian, J., Zhang, C. & Wang, F. Explaining Algorithmic Fairness through Fairness-Aware Causal Path Decomposition. In *Proceedings of the ACM SIGKDD International Conference on Knowledge Discovery and Data Mining*, DOI: [10.1145/3447548.3467258](https://doi.org/10.1145/3447548.3467258) (2021).
22. Castelnovo, A. *et al.* A clarification of the nuances in the fairness metrics landscape. *Sci. Reports* **12**, DOI: [10.1038/s41598-022-07939-1](https://doi.org/10.1038/s41598-022-07939-1) (2022).
23. Dwork, C., Hardt, M., Pitassi, T., Reingold, O. & Zemel, R. Fairness through awareness. In *ITCS 2012 - Innovations in Theoretical Computer Science Conference*, DOI: [10.1145/2090236.2090255](https://doi.org/10.1145/2090236.2090255) (2012).
24. Kleinberg, J., Mullainathan, S. & Raghavan, M. Inherent trade-offs in the fair determination of risk scores. In *Leibniz International Proceedings in Informatics, LIPIcs*, vol. 67, DOI: [10.4230/LIPIcs.ITCS.2017.43](https://doi.org/10.4230/LIPIcs.ITCS.2017.43) (2017).
25. Singer, M. *et al.* The third international consensus definitions for sepsis and septic shock (sepsis-3), DOI: [10.1001/jama.2016.0287](https://doi.org/10.1001/jama.2016.0287) (2016).
26. Jones, A. E., Trzeciak, S. & Kline, J. A. The Sequential Organ Failure Assessment score for predicting outcome in patients with severe sepsis and evidence of hypoperfusion at the time of emergency department presentation. *Critical Care Medicine* **37**, DOI: [10.1097/CCM.0b013e31819def97](https://doi.org/10.1097/CCM.0b013e31819def97) (2009).
27. Groenwold, R. H. H. Informative missingness in electronic health record systems: the curse of knowing. *Diagn. Progn. Res.* **4**, DOI: [10.1186/s41512-020-00077-0](https://doi.org/10.1186/s41512-020-00077-0) (2020).
28. Vincent, J. L. *et al.* The SOFA (Sepsis-related Organ Failure Assessment) score to describe organ dysfunction/failure. *Intensive Care Medicine* **22**, DOI: [10.1007/BF01709751](https://doi.org/10.1007/BF01709751) (1996).
29. Smith, G. B., Prytherch, D. R., Meredith, P., Schmidt, P. E. & Featherstone, P. I. The ability of the National Early Warning Score (NEWS) to discriminate patients at risk of early cardiac arrest, unanticipated intensive care unit admission, and death. *Resuscitation* **84**, DOI: [10.1016/j.resuscitation.2012.12.016](https://doi.org/10.1016/j.resuscitation.2012.12.016) (2013).
30. Machado, F. R. *et al.* Getting a consensus: Advantages and disadvantages of Sepsis 3 in the context of middle-income settings, DOI: [10.5935/0103-507X.20160068](https://doi.org/10.5935/0103-507X.20160068) (2016).
31. Breiman, L., Friedman, J. H., Olshen, R. A. & Stone, C. J. *Classification and regression trees* (Chapman & Hall/CRC, 2017).
32. Chipman, H. A., George, E. I. & McCulloch, R. E. Bayesian CART model search. *J. Am. Stat. Assoc.* **93**, DOI: [10.1080/01621459.1998.10473750](https://doi.org/10.1080/01621459.1998.10473750) (1998).
33. Yang, M. *et al.* Early Prediction of Sepsis Using Multi-Feature Fusion Based XGBoost Learning and Bayesian Optimization. In *2019 Computing in Cardiology Conference (CinC)*, vol. 45, DOI: [10.22489/cinc.2019.020](https://doi.org/10.22489/cinc.2019.020) (2019).
34. Chen, T. & Guestrin, C. XGBoost: A scalable tree boosting system. In *Proceedings of the ACM SIGKDD International Conference on Knowledge Discovery and Data Mining*, vol. 13-17-August-2016, DOI: [10.1145/2939672.2939785](https://doi.org/10.1145/2939672.2939785) (2016).
35. Bergstra, J., Bardenet, R., Bengio, Y. & Kégl, B. Algorithms for hyper-parameter optimization. In *Advances in Neural Information Processing Systems 24: 25th Annual Conference on Neural Information Processing Systems 2011, NIPS 2011* (2011).